PROCEEDINGS, 46th Workshop on Geothermal Reservoir Engineering
Stanford University, Stanford, California, February 16-18, 2021
SGP-TR-216

Delineating Faults at the Soda Lake Geothermal Field Using Machine Learning

Kai Gao[1], Lianjie Huang[1], Rongrong Lin[2], Hao Hu[2], Yingcai Zheng[2], Trenton Cladohous[3]

[1]Geophysics Group, Los Alamos National Laboratory, Los Alamos, NM 87545, USA; [2] Department of Earth and Atmospheric Sciences, University of Houston, TX 770043, USA; [3]Cyrq Energy, Inc., 4010 Stone Way North, Suite 400, Seattle, WA 98103, USA

kaigao@lanl.gov; ljh@lanl.gov

Keywords: Fault, fault detection, geothermal, machine learning, seismic interpretation

ABSTRACT

Accurate fault detection on seismic images is one of the most important and challenging tasks in the field of automatic seismic interpretation. Conventional human-picking and semi-human-intervened fault detection approaches are being replaced by fully automatic methods thanks to the development of machine learning. We develop a novel machine learning-based fault detection approach using a multiscale connection-fusion U-shaped convolutional neural network (MCFU for short). The most important characteristics of our MCFU method is that it uses skip connections to connect feature maps of different spatial resolutions, and uses a fusion operation to generate the final fault map. This architecture enables our MCFU to fully use spatial information embedded in the feature maps. We demonstrate through seismic migration images from the Soda Lake geothermal field that our MCFU produces cleaner, more interpretable fault maps for complex seismic images compared with the ant-tracking method that is widely used in industry, and with the conventional U-shaped convolutional neural network, thus leading to potentially improved geologic interpretability of detected faults.

1. INTRODUCTION

Faults are usually observed as planar displacements in subsurface rocks. Geologically, faults result from local to regional stress-induced brittle failure that eventually leads to visible displacement of rock formations along a fault plane (Fossen, 2016). Faults are geologically important because they are usually the key to inferring the stress or strain environment evolution. Faults play a crucial role in geothermal energy exploration. In hydrogeothermal systems, connected fault systems act as pathways for geothermal fluid injection, flow, and heat extraction; therefore, reliable fault detection is imperative to optimizing well placement for maximizing geothermal energy production (Gan Elsworth, 2014; Gao et al., 2020).

Seismic interpretation is marching quickly into a new era thanks to the advancement of machine learning. Of all seismic interpretation tasks, automatic fault detection based on machine learning achieves notably superior outcomes compared with conventional paradigms. Wu et al. (2019) developed an end-to-end fault detection method based on convolutional neural network (CNN) (LeCun et al. 1998), or U-Net precisely. The method of Wu et al. (2019) is a simplified version of the U-Net developed initially for image segmentation (Ronneberger et al., 2015). In neural network architecture, the U-Net is a special type of CNN that contains an encoding branch and a decoding branch. Specifically, different from rudimentary CNNs where the input sequentially flows through convolutional layers, U-Net employs a series of so-called skip connections to convey location information between the encoder branch and the decoder branch in addition to simple downsampling or upsampling within each branch. These pairs of convolutional layers connected by skip connections have different "distances," i.e., a highest-level encoder layer has a skip connection with a highest-level decoder layer, and a lower-level encoder layer has a skip connection with a lower-level decoder layer, etc., making the CNN visually a U-shaped neural network concatenated by long/short skip connections between the encoder/decoder branches. Notably, a skip connection connects a pair of encoder/decoder layers at the same resolution level. Wu et al. (2019) demonstrated that the U-Net-based approach provides superior detection accuracy along with significantly improved computational efficiency compared with conventional attribute-based approaches. Di et al. (2019) incorporated geological information into CNN to produce fault maps with improved geological interpretability of detected faults. Methods that focus on reducing the necessary amount of training data/labels are also reported in recent works (Cunha et al., 2020).

We develop a novel fault-detection approach based on a multiscale connection-fusion U-shaped CNN (MCFU for short). Our work translates recent developments of U-Net derived image segmentation, particularly U-Net 3+ (Huang et al., 2020), into seismic fault detection. Yet we incorporate important simplifications, modifications, and improvements based on these prior works, and design a novel CNN architecture for fault detection on seismic migration images. Our approach is an improved version of U-Net for automatic, end-to-end fault detection. Specifically, in contrast to the U-Net that uses only same-level skip connections to convey spatial information between encoder/decoder feature maps, our MCFU employs additional skip connections to connect feature maps of different levels. In our MCFU, skip connections also exist within the decoder branch. In addition, our MCFU generates independent fault maps at different spatial scales and subsequently employs a series of fusion operation to generate the final high-resolution fault map. We demonstrate using several synthetic and real seismic image examples that these two important features enable MCFU to generate a fault map with notably cleaner, more continuous faults compared with the U-Net, thus leading to improved fault interpretability on MCFU-generated fault maps.

2. METHODOLOGY

Our multiscale connection-fusion U-Net (MCFU) uses a more complex architecture compared with conventional U-Net CNN. We display the overall structure of our MCFU in Figure 1.

Similar to the U-Net, our MCFU consists of an encoder branch and a decoder branch, each with several levels. Specifically, we use four encoders and three decoders. In conventional U-Net, the skip connection connects a pair of encoder and decoder at the same level to transfer segmentation information through the entire neural network, i.e., encoder 1 connects only with decoder 1 through a concatenation, encoder 2 connects only with decoder 2 with a concatenation, etc. In MCFU, in addition to same-level skip connections, we also connect encoders/decoders at different levels using skip connections, indicated by the black, blue, and red color connection lines in Figure 1. In MCFU, each decoder connects with all encoders with these long/short skip connections. Therefore, each decoder has spatial information from different levels in the neural network, leading to more accurate spatial information constraints and transfer the information among different levels. In this sense, MCFU is a multiscale connected U-Net.

Another distinct feature of our MCFU compared with the U-Net is that, at each of the four resolution levels, we produce an independent fault map output, and merge these four outputs into a final fault map after proper upsampling and convolution operations. We use horizontal red arrows to indicate this fusion operation, where we use the sigmoid activation function along with a 1-by-1 kernel size in the convolution. The final fault map output is what we use in the training against the ground-truth fault map (i.e., the training label). It contains fused fault location information provided by the four fault maps of different spatial resolutions. This is slightly different from imposing supervisions on all four independent fault maps as in U-Net 3+ (Huang et al., 2020). In this perspective, MCFU is a multiscale fusion U-Net.

The multiscale connection-fusion architecture indicates that our MCFU contains three subnets shown in Figure 2a-c. The three subnets are similar to one another in connection patterns. We take the subnet associated with decoder 2 shown in Figure 2b as an example to illustrate the construction of MCFU subnets.

In the subnet associated with decoder 2, we first create an intermediate convolutional layer by concatenating the convolutional layers produced by either downsampling or upsampling encoder/decoder layers. For concatenation, these encoder/decoder layers should have the same width and height (i.e., the dimensions other than the concatenation axis). Therefore, we employ the following procedure to generate decoder 2:

(1) Downsample encoder 1 using a max-pooling layer of ratio 2-by-2 plus a convolutional layer with a 3-by-3 kernel and 32 channels;
(2) Convolve encoder 2 using a convolutional layer with a 3-by-3 kernel and 32 channels;
(3) Upsample encoder 3 using a bilinear interpolation of size 2-by-2 plus a convolutional layer with a 3-by-3 kernel and 32 channels;
(4) Upsample encoder 4 using a bilinear interpolation of size 4-by-4 plus a convolutional layer with a 3-by-3 kernel and 32 channels; and then
(5) Convolve this concatenation layer with a convolutional layer with a 3-by-3 kernel and 64 channels equipped with a rectified linear unit (ReLU) activation function, and finally batch-normalize the output.

We use a similar procedure to construct decoders 1 and 3 as shown in Figures 2a and c, respectively. Note that in both encoders and decoders, our architecture is slightly different from that of the U-Net 3+. In encoders, for example, we use two convolutional layers with the same number of feature maps (or depth). For decoders at different levels, we use different numbers of feature maps, and the number of feature maps in a decoder is consistent with that in the encoder at the same level. Thus, our MCFU is more symmetric in the feature map number at different spatial resolution scales compared with U-Net 3+.

In summary, our MCFU distinguishes itself from the U-Net in two aspects: First, MCFU connects all encoders and decoders with skip connections of different levels, thus can more accurately preserve fault location information for fault detection; Second, MCFU outputs four fault maps of different resolutions, and merges them to produce a final high-resolution fault map with an additional convolutional layer, and thus can effectively ensure that the fault maps at different spatial resolution scales are all accurate, instead of only at the highest resolution scale as in the U-Net. We demonstrate through numerical examples that these two features enable our MCFU to produce cleaner, more accurate fault maps compared with the U-Net on complex seismic images.

3. RESULTS

Figure 3a shows a 2D P-wave velocity model built using geological features of the Soda Lake geothermal field (Gao et al., 2020). We use red dashed lines to indicate the positions of three major faults in the horizontal center. These three faults are implicitly superimposed onto the velocity model when we built the velocity model, i.e., they appear as weak lateral velocity changes in the model instead of explicit faults. Several other faults are similarly built into the model. Figure 3b shows a 2D seismic image produced using a vector elastic reverse-time migration method (Gao and Huang, 2019). The dimension of the seismic image is 256 grid points in the vertical direction and 512 grid points in the horizontal direction, with actual physical dimensions of 0.6 km by 3.4 km. We process the image using a nonlinear anisotropic diffusion filtering to improve the visibility of faults for our fault-detection test purpose.

We first perform fault detection using the ant-tracking module of Schlumberger's Petrel software suite, and display the result in Figure 4a. The ant-tracking fault-detection method is the state-of-the-art technique widely used in industry. The method finds almost every visible “faults” on the image, yet there exist two major issues. First, the fault probability associated with these detected faults is low with an average value of approximately 0.3 to 0.4. Second, there exist some obvious erroneous detections. For example, at the center of the image, the method produces two high-probability, yet wrong faults with low dips. On the right part of the image, we also find that some predicted faults are parallel with sedimentary reflectors, which are obviously incorrect.

We then perform two detections using the U-Net and our MCFU, and show the results in Figure 4b and c, respectively. Both methods produce a fault map with almost every possible fault delineated. Nevertheless, it is visually evident that some faults detected by our

MCFU are different from those detected by the U-Net. Overall, our MCFU produces a visually cleaner fault map with fewer misidentifications. For example, in the horizontal center region of the image, there exists a vertical fault spanning from the surface to the top of the basalt body. The U-Net detects this fault, yet the bottom part of the detected fault obviously bends and finally merges with a fault to its right. By contrast, our MCFU produces a more reliable prediction – a nearly vertical fault. Our MCFU also produces fewer artifacts in the predicted fault map. For instance, at the horizontal position of approximately 2.5 km, there exist some isolated artifacts on the U-Net fault map, which are unlikely to be any types of faults. By contrast, our MCFU produces a notably cleaner fault map for this region. The faults predicted by our MCFU at the horizontal position of approximately 1.3 km and above the top of the basalt body are also cleaner compared with those produced by the U-Net.

To further evaluate the accuracy of our MCFU, we perform another three fault detections on a 2D seismic image in Figure 5 generated using field seismic data from the Soda Lake geothermal field. We process the image using a windowed 2D root-mean-square balancing, along with a mild nonlinear anisotropic diffusion filtering to enhance reflectors. Figures 6a-c show the fault detection results produced using Petrel's ant-tracking module, the U-Net, and our MCFU, respectively. The comparison resembles that for the synthetic image shown in Figure 4. The two neural network methods obviously outperform the ant-tracking approach in both detection accuracy and fault interpretability. In addition, our MCFU provides a slightly better prediction where the faults have an improved horizontal resolution compared with the U-Net. Our MCFU also produces a more accurate prediction on some small-scale faults, e.g., the one at the horizontal position of 3.6 km, and some unusual fault structures, such as the two nearly intersecting faults at the horizontal position of approximately 2.6 km. Overall, our MCFU provides the most interpretable fault map among the three methods.

4. CONCLUSIONS

We have developed a novel fault detection method using a multiscale connection-fusion convolutional neural network. The neural network makes use of multiscale skip connections between encoders and decoders at different spatial resolution scales, along with a multiscale fusion approach, to produce high-resolution fault maps from seismic migration images. We demonstrate the superior fault-detection capability of our method compared with the ant-tracking method that is widely used in industry, and the current state-of-the-art U-Net architecture fault detection method, using a 2D seismic image from the Soda Lake geothermal field. Future work aims at training the neural network for 3D fault detection.

5. ACKNOWLEDGMENTS

This work was supported by the U.S. Department of Energy (DOE) Geothermal Technologies Office through the Los Alamos National Laboratory (LANL). LANL is operated by Triad National Security, LLC, for the U.S. DOE National Nuclear Security Administration (NNSA) under Contract No. 89233218CNA000001. This research used computing resources provided by the LANL Institutional Computing Program supported by the U.S. DOE NNSA under Contract No. 89233218CNA000001.

REFERENCES

Fossen, H., 2016, Structural Geology, 2 ed.: Cambridge University Press.

Hardman, R. F. P., and J. E. Booth: The significance of normal faults in the exploration and production of North Sea hydrocarbons: Geological Society, London, Special Publications, 56, no. 1, 1–13, (1991)

Gan, Q., and D. Elsworth: Analysis of fluid injection-induced fault reactivation and seismic slip in geothermal reservoirs: Journal of Geophysical Research: Solid Earth, 119, no. 4, 3340–3353, (2014)

Gao, K., L. Huang, and T. Cladouhos: Three-dimensional seismic characterization and imaging of the Soda Lake geothermal field: Geothermics, 101996, (2020)

Vilarrasa, V., and J. Carrera: Geologic carbon storage is unlikely to trigger large earthquakes and reactivate faults through which CO2 could leak: Proceedings of the National Academy of Sciences, 112, no. 19, 5938–5943, (2015)

Wu, X., L. Liang, Y. Shi, and S. Fomel: FaultSeg3D: Using synthetic data sets to train an end-to-end convolutional neural network for 3D seismic fault segmentation: Geophysics, 84, no. 3, IM35–IM45, (2019)

LeCun, Y., L. Bottou, Y. Bengio, and P. Haffner: Gradient-based learning applied to document recognition: Proceedings of the IEEE, 86, no. 11, 2278–2324, (1998)

Ronneberger, O., P. Fischer, and T. Brox: U-Net: Convolutional networks for biomedical image segmentation: Proceedings of Medical Image Computing and Computer-Assisted Intervention, 234–241, (2015)

Di, H., C. Li, S. Smith, and A. Abubakar: Machine learning-assisted seismic interpretation with geologic constraints: SEG Technical Program Expanded Abstracts, 5360–5364, (2019)

Huang, H., L. Lin, R. Tong, H. Hu, Q. Zhang, Y. Iwamoto, X. Han, Y.-W. Chen, and J. Wu: UNet 3+: A full-scale connected UNet for medical image segmentation: arXiv:2004.08790, (2020)

Cunha, A., A. Pochet, H. Lopes, and M. Gattass: Seismic fault detection in real data using transfer learning from a convolutional neural network pre-trained with synthetic seismic data: Computers & Geosciences, 135, 104344, (2020)

Gao, K., and L. Huang: An efficient vector elastic reverse time migration method in the hybrid time and frequency domain for anisotropic media: Geophysics, 84, no. 6, S511–S522, (2019)

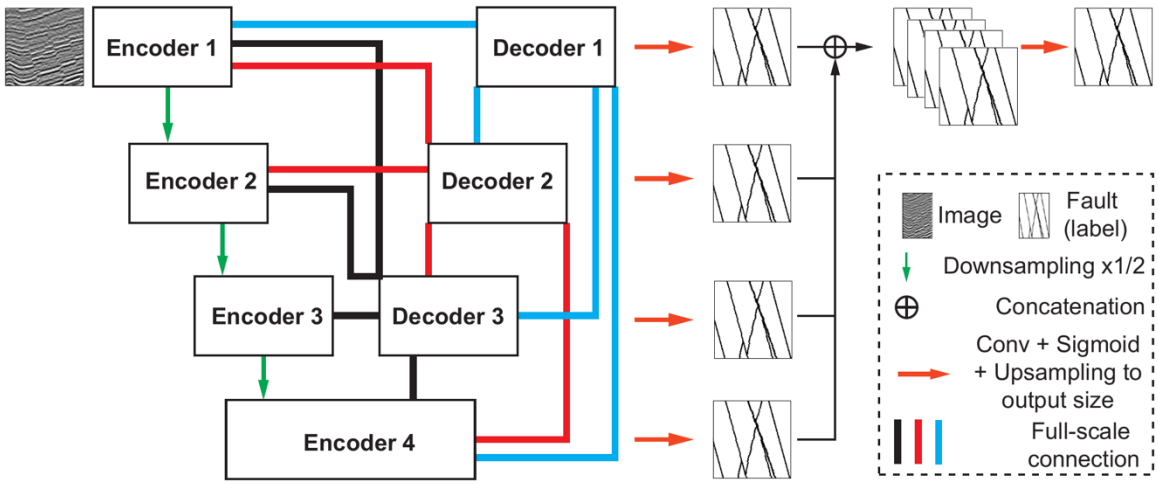

Figure 1: The overall architecture of our MCFU. The input is a 2D or 3D seismic image, and the output is a same-size fault probability map with a value range from 0 to 1.

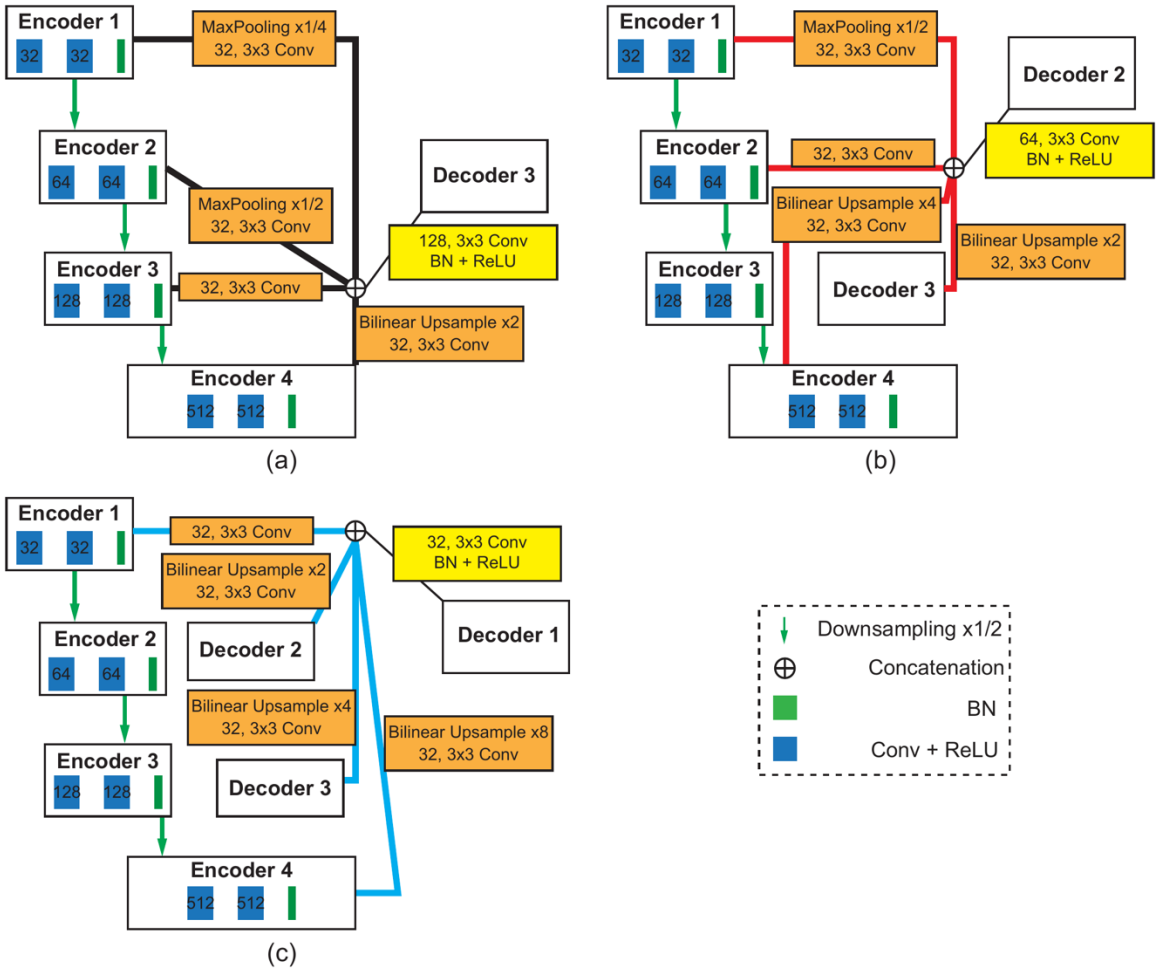

Figure 2: The three embedded subnets in our MCFU. Panels (a)-(c) represent the subnets associated with decoders 1, 2, and 3, respectively. BN represents batch normalization. ReLU represents the rectified linear unit activation function in the convolutional operation. Operations prior to concatenations in each subnet are explained in orange-colored rectangles.

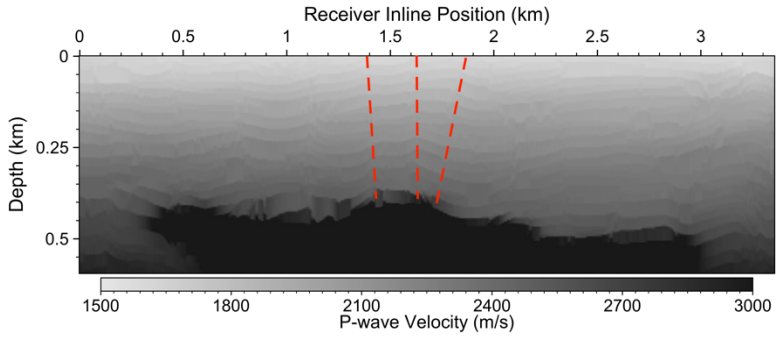

(a)

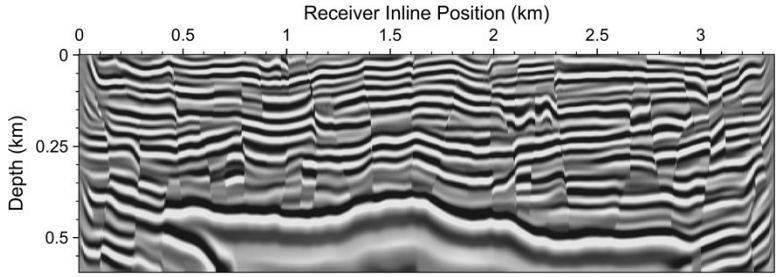

(b)

Figure 3: (a) A 2D velocity model built using geological features of the Soda Lake geothermal field, with red dashed lines indicating three of the many implicit faults superimposed onto the model during model building. (b) A 2D seismic image produced using vector elastic reverse-time migration of synthetic surface seismic data for the velocity model in (a). The maximum value of the P-wave velocity in (a) is 4,800 m/s. We display the model with an upper clip value of 3,000 m/s for visualization purpose.

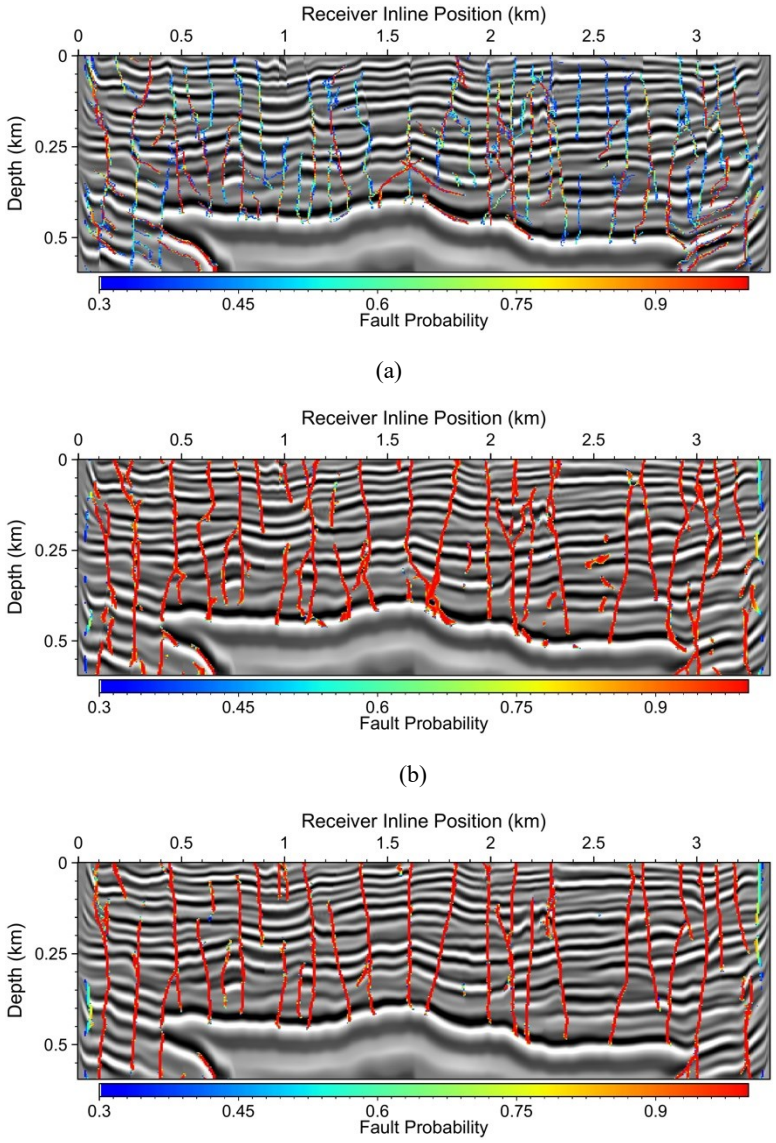

Figure 4: Panels (a)-(c) show the detected faults overlying on the image obtained using Petrel's ant-tracking fault detection module, the U-Net, and our MCFU, respectively.

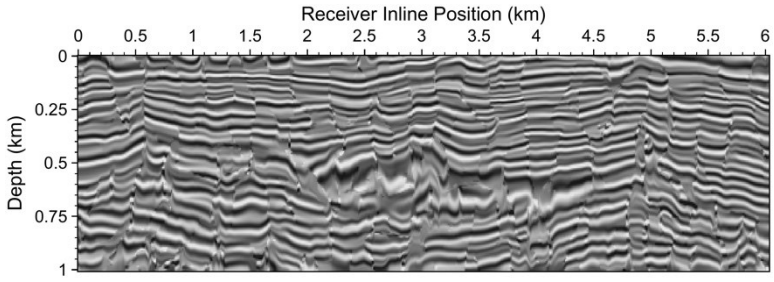

Figure 5: A processed 2D seismic image sliced from the 3D migration image volume of the Soda Lake geothermal field produced using 3D field surface seismic data (Gao et al., 2020).

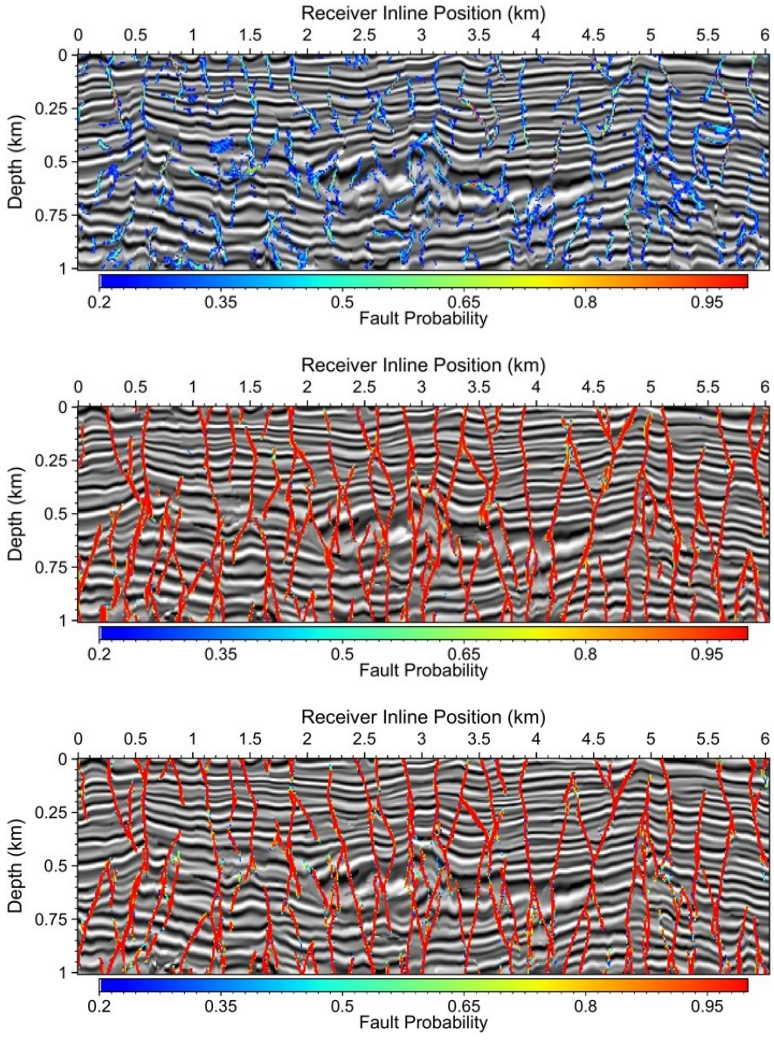

Figure 6: Fault detection results generated using (a) Petrel's ant-tracking module, (b) the U-Net, and (c) our MCFU, respectively.